Using Transmissive Photonic Band Edge Shift to Detect Explosives – A Study with 2,4,6-trinitrotolune (TNT)

Noorhayati Idros [1,2] , Man Yi Ho [1,3] , Varun S. Kamboj [4] , Hua Xu [5] , ZhongZe Gu [5] , Harvey E. Beere [4] , David A. Ritchie [4] , Daping Chu [1*]

[1]   Electrical Engineering Division, Engineering Department, University of Cambridge, Cambridge, CB3 0FA, United Kingdom.

[2]   Institute of Nano Electronic Engineering (INEE), Universiti Malaysia Perlis (UniMAP), Lot 106, 108 & 110, Tingkat 1, Block A, Taman Pertiwi Indah, Jalan Kangar-Alor Setar, Seriab 01000 Kangar, Perlis, Malaysia.

[3]   Schlumberger Cambridge Research, High Cross, Madingley Road, Cambridge, CB3 0EL, United Kingdom.

[4]   Cavendish Laboratory, Physics Department, University of Cambridge, Cambridge, CB3 0HE, United Kingdom.

[5]   State Key Laboratory of Bioelectronics, School of Biological Science and Medical Engineering, Southeast University, 2 Sipailou, Nanjing, 210096, China.

Corresponding Author

*   Author to whom correspondence should be addressed; E-Mail: dpc31@cam.ac.uk; Tel.: +44 (0) 1223 748352; Fax: +44 (0) 1223 748342

ABSTRACT Photonic crystals (PhCs) possess outstanding optical properties that can be exploited for chemical sensing. We utilized a three-dimensional close-packed PhC structure made of functionalized silica nanoparticles. They consist of alternating high and low refractive index regions and has optical properties, such as photonic band structures, that are very sensitive to the change of physical structures. This study use 2,4,6-trinitrotolune (TNT) to illustrate a detection method based on the transmissive photonic band edge shift (TPBES) due to the binding of TNT with amine anchored on particle surfaces to form Meisenheimer (amine-TNT) complexes. PhCs are exceptionally sensitive to a small change in refractive index caused by surface modification. As a result, it is suitable for sensing specific reactions between amine and TNT. This method achieved a wide detection range of TNT concentrations from 10^{-12} M to 10^{-4} M. 2,4-dinitritoluene (DNT) and toluene were used as a control and blank, respectively. Because of gravitational sedimentation, the TNT-functionalized particles were self-assembled in pure ethanol. They were measured by UV-Visible transmission spectroscopy. A three-dimensional model to simulate the detection system was built using the particles centre-to-centre distance (a) and effective dielectric constant (ε) as a function of the TNT concentrations. Two sets of simulations were performed: the first set involved a parametric sweep of the centre-to-centre distance of TNT functionalized crystals using $\varepsilon = 2.015$. The second set involved a parametric sweep of the dielectric constant with $a = 263.1$ nm. These perturbations yield a TPBES response that is in agreement with our experimental results.

KEYWORDS: Transmission, photonic crystal, nano particles, self-assembly, TNT

Photonic crystals (PhCs) are periodic arrangements of regularly shaped materials with different dielectric constants.[1] The material is engineered such that only light of a certain wavelength can propagate through the lattice of this arrangement.[2] Yablonovitch and John undertook the first detailed research on engineered PhCs.[3-4] The periodicity of PhCs can vary from a single-dimensional (1D) to a three-dimensional (3D) structure depending on its applications. Fabrication of 1D and 2D PhCs are mostly prepared by conventional lithography techniques such as photolithography, multiple spin coating, layer-by-layer deposition, and etching.[5-8]

3D PhCs however, can be produced by cheaper techniques such as self-assembly of nanoscopic, monodisperse spheres into a photonic crystal host simply known as colloidal self-assembly.[9-10] Normally such spheres consist of dielectric materials, for example, silica, titanium dioxide, zinc oxide, or organic polymers including poly(methyl methacrylate) and polystyrene.[11-18] Colloidal self-assembly offers a means of low-cost production of 3D photonic crystals with a large surface area[19-20] and which exhibit a complete photonic bandgap. The combination of these two factors enables these crystals to manipulate light in 3D space.[10] Photonic bandgaps (PBGs) forbid propagation of electromagnetic waves of certain frequency ranges. The optical properties of PBG structures are highly sensitive to the thickness and refractive index of their constituents. Small changes in the refractive index of PBG structures due to the capturing of external stimuli[1] such as a ligand-receptor interaction can be detected as shifts in the reflectance spectrum.[21]

Colloidal mesoporous such as silica nanoparticles have several benefits: they offer a large sensing surface area; they available to integrate functional groups; and they are capable of immobilizing into an inorganic mesopores network with active molecules.[22–29] In addition, the mesoporous particles in suspension can stay suspended over a long period of time, making them ideal for surface coatings.[30] Colloidal mesoporous nanoparticles have found promising applications in the fluorogenic detection of nitroaromatic explosives such as luminescent colloidal oligo(tetraphenyl)silole nanoparticles in THF/H_2O suspensions[31], nanoscopic-capped mesoporous hybrid materials or MCM-41 support[32], and silica mesoporous supports gated with tetrathiafulvalene derivatives.[33] Xu and Lu[34] developed a M-MIPs@CDs fluorescence sensor for detection of 2,4,6-trinitrotoluene (TNT) with sensitivity of 17 nM. Liu and Chen[35] also reported detection of TNT with sensitivity of 10^{-11} M using graphene nanosheet-supported silver nanoparticles. The reported fluorescence sensors involved complex analytical instrumentations

and expensive materials. However, in this proposed transmissive photonic band edge shift (TPBES) based detection of TNT offers an attractive option for a much simpler, inexpensive, convenient and label-free alternative[1] with excellent sensitivity of pM.

Sensing of trace explosives such as TNT is a complex and challenging task due to the lack of inexpensive sensors with high selectivity and sensitivity[36], the lack of easily detectable signals, and wide selection of explosive compositions.[37,38] Furthermore, explosive-based terrorism has grown rapidly in recent years, causing enormous damage to public safety and environmental pollution. These explosive-based weapons can be deployed in simple and variety of schemes. [39-41] Primarily used nitroaromatic explosives produced during military preparation of landmines[42-47], TNT is also one of the key sources of dangerous water contamination,[48] as well as being toxic to aquatic creatures. Exposure to TNT may cause pancytopenia, a disorder of the blood-forming tissues in humans and other mammals.[49] Thus, developing a practical analytical method to monitor TNT is pressing and crucial to solving these problems.

We propose a method to detect TNT by anchoring the SiO_2 nanoparticles surface with amine (—NH_2) head groups from 3-aminopropyl-triethoxysilane (APTES) that act as bioreceptors that selectively bind with TNT targets. This method is very selective and simpler than the two-step reactions reported in our previous findings[50] since we have confirmed that APTES has an excellent selectivity with TNT. The formation of the amine-TNT or Meisenheimer complexes is attributed to the strong acceptor-donor interaction between the nitro group of TNT and amine respectively.[51.52] Figure 1 shows the molecular schematic of the complex.
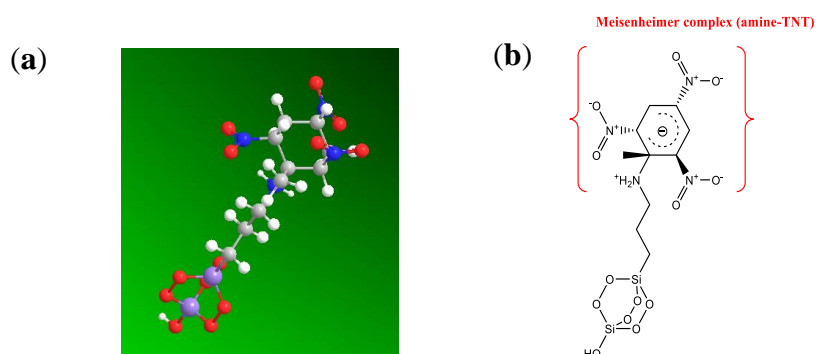

Figure 1. Molecular schematic of the Meisenheimer complex: (**a**) Ball and stick three-dimensional representation. The 3D structure represents oxygen, hydrogen, nitro, carbon and silicon atoms as red, white, blue, gray and purple balls respectively. (**b**) Chemical structure representation of the Meisenheimer (amine-TNT) complex functionalized onto the SiO_2 crystal.

The surface functionalization scheme is demonstrated in Figure 2. As a result of ligands binding, the nanoparticle separation increased from state 1 to 3 (a_0 to a_2). An increase in the TNT concentrations further increase the effective particle separation and the contrast of the refractive index of the functionalized system.
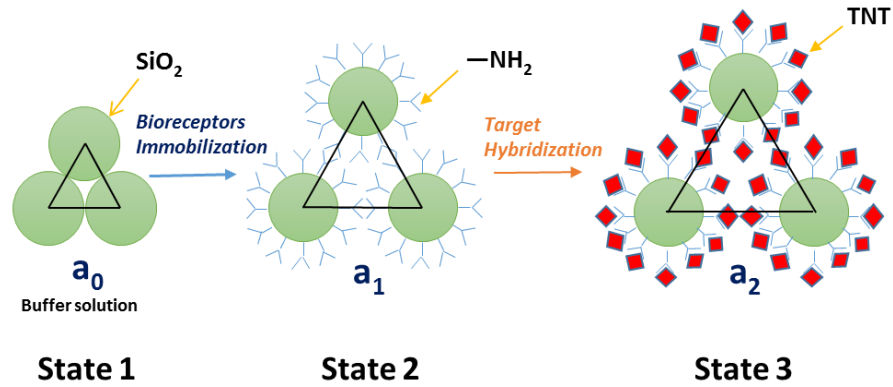

Figure 2. Surface functionalization of silica particles: the separation between the close-packed particles increases from state 1 to 3 (a_0 to a_2).

Self-assembly of the functionalized nanoparticles forms a closely-packed structure that can be observed under scanning electron microscopy. Because of gravitational sedimentation, the TNT-functionalized particles were self-assembled in pure ethanol. This sedimentation structure is shown in Figure 3. The settled structure was measured by UV-Visible transmission spectroscopy. From the measurement, three regions of high and low transmittance were observed. The high and low transmittance edges are the respective photonic band (PB) and band gap (PBG) edges.
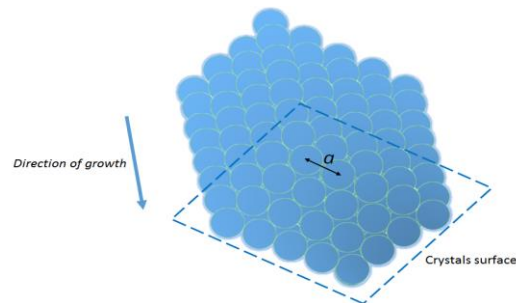

Figure 3: Self-assembled structure of functionalized TNT particles under gravity force.

TPBES response measures the normalized frequency calculated as the particles centre-to-centre distance *(a)* divided by the measured wavelength *(λ),* as a function of TNT concentrations. A wide detection range of TNT concentrations was used and successfully detected from 10^{-12} M to 10^{-4} M together with 2,4-dinitritoluene (DNT) and toluene as control and blank, respectively. The TPBES system is very selective towards TNT even though the chemical structure of TNT and DNT are relatively similar as shown in Figure 4. Apart from the outstanding selectivity between amine and TNT, the effective particle separation (*a*) increased with the TNT concentration and changed the contrast of the refractive index (n_{eff}) which resulted in the PB and PBG edge shifts. Successful detection of TNT is caused by a periodic arrangement of the functionalized crystals. On the other hand, an incomplete reaction between DNT and amine resulted in randomization of their self-assembly structure. This randomization effect resulted in decreasing signals of TPBES response with no distinctive photonic bands and band gaps shown in the results section.
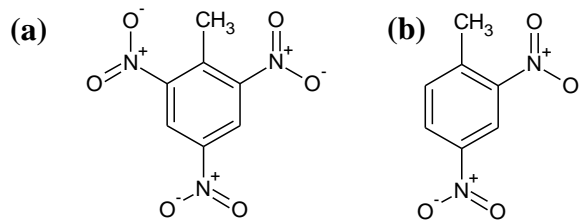

Figure 4: Explosive structures of (a) TNT and (b) DNT.

A three-dimensional model to simulate the detection system was built using the particles centre-to-centre distance (*a*) and effective dielectric constant (*ε*) as a function of the TNT concentrations. Two sets of simulations were performed: the first set involved a parametric sweep of the centre-to-centre distance of TNT functionalized crystals using *ε* = 2.015; the second set involved a parametric sweep of the dielectric constant with *a* = 263.1 nm. The perturbations of the centre-to-centre distance and dielectric constant yield a TPBES response as described by Equation (i) in the result section. We observed that the simulation results are in agreement with our experimental results that are further described in the results section.

This detection method reveals band edges sharper than reported in our previous findings[50] with full penetration of light through the three-dimensional self-assembly structure. A combined effect of the high surface area-to-volume ratio of the functionalized nano particles in use and the

full penetration of the light through the assembled structure, helped to expand the dynamic range of the detection from 10^{-12} to 10^{-4} M. The method presented in this study offers a convenient tool for label-free sensing, since the effect can be made specific for TNT, and can be incorporated easily into microfluidic systems.

Results

Transmissive Photonic Band Edge Shift. The transmission spectrums for bare silica and amine-functionalized crystals are illustrated in Figure 5 (a) (i) and (ii), respectively. They exhibit sharp band edges which consist of three high and low regions that correspond to respective photonic band and band gaps. A photonic band edges are the edges of the high normalized frequencies, calculated as the particles centre-to-centre distance (a) divided by the measured wavelength (λ). The shifts in the photonic bands (PBs) and band gaps (PBGs) for bare silica and amine-functionalized crystals are plotted in Figure 5 (b).

The shift is caused by an increased in the average centre-to-centre distance (a) from 250.2 nm to 257.7 nm, measured by scanning electron microscopy (SEM). Sampling on the transmission of 10^{-4} M TNT as seen in Figure 5 (c) exhibits sharper edges in comparison to the reflection signal and other TNT-detection configurations[30, 53-58]. These edges provide an accurate indication of the bands with small measurement error in the whole composition range.

From an applied standpoint, TPBES response offers a better detection system than its counterpart for of the following reasons. Firstly, the reflection technique is limited only to the light interaction on the crystals surface than the overall three-dimensional penetration of the assembled structure seen by the transmitted lights.

Secondly, the arrangement of packed crystals from the gravity sedimentation method[59-60] used to grow the reflection films is restricted by their low mobility on the bottom substrate when the gravity force surpasses the Brownian motion or interparticle electrostatic repulsion. Thus, the resultant self-assembled crystals are considerably less ordered, and they exhibit poor assembly efficiency in particularly on the surface. Cracks regularly occur upon drying due to the tensile stress arising from the capillary-force-induced shrinkage of the pre-assembled array against a rigid substrate[61].
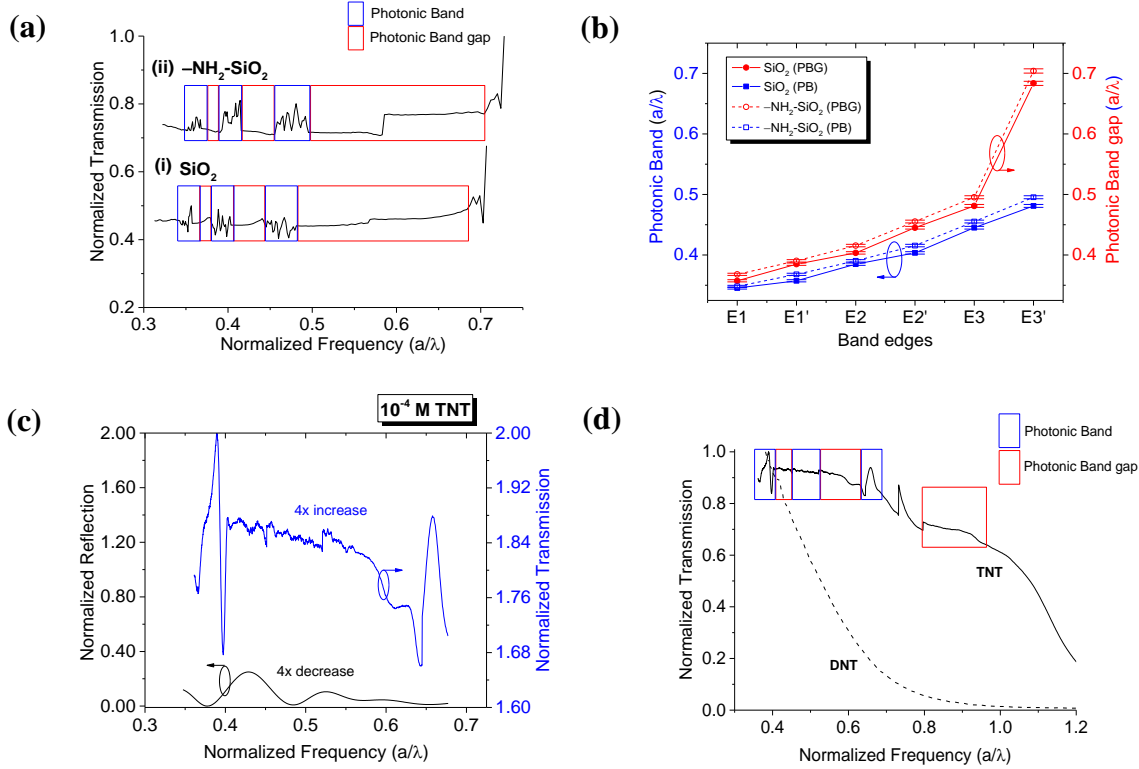
Figure 5. Transmissive Photonic Band Edge Shift: (**a**) Normalized transmission against normalized frequency (a/λ) of (**i**) SiO_2 and (**ii**) —NH_2-SiO_2. (**b**) The corresponding TPBES response of photonic band and band gap edges before and after amine functionalization. (**c**) For the sake of contrast, sampling on the normalized reflection (with signal decreased by four times) exhibit edges less sharp in comparison to the normalized transmission (with signal increased by four times). (**d**) The TPBES responses of 10^{-4} M TNT and DNT functionalized crystals.

TPBES crystals assembled in solution achieve equilibrium between stabilizing and destabilizing factors of gravity, of the respective Brownian motion and interparticle forces. Due to these reasons, the structure of the TPBES crystals may have higher regularity as a whole than the structure obtained in the reflection side.

The increase of TNT concentrations from 10^{-12} M to 10^{-4} M further increased the effective particle separation as shown in Table 1. This is because successful detection of TNT on the amine-functionalized crystals (—NH_2-SiO_2) surfaces resulted in a periodic arrangement of the functionalized crystals. Figure 6 (a) and (b) are the SEM images of the respective structures of —

NH$_2$-SiO$_2$ and 10^{-4} M TNT-functionalized crystals. The centre-to-centre distance of crystals increased from 257.7 nm of the —NH$_2$-SiO$_2$ to 270.9 nm after 10^{-4} M TNT functionalization.

Table 1. Average center-to-center distance, (*a*) of functionalized crystals measured by scanning electron microscopy for different TNT concentrations.

Concentration of TNT (M)	Centre-to-centre distance (nm)
10^{-12}	263.1
10^{-10}	265.4
10^{-8}	266.0
10^{-6}	267.2
10^{-4}	270.9

An incomplete reaction between DNT and —NH$_2$-SiO$_2$ crystals[50] resulted in randomization of their self-assembly structures as shown in Figure 6 (c). Using SEM measured only on uniform crystal areas, the centre-to-centre distance of the 10^{-4} M DNT-crystals is approximated to be 286 nm. However, this value does not represent the entire sample because of the randomization effect.

The randomization of DNT crystals resulted in decreasing signals of its TPBES response shown in Figure 5 (d) with no distinctive photonic bands and band gaps. The approximated centre-to-centre distance of the DNT-crystals was used in order to compare the TPBES response between 10^{-4} M TNT- and the control DNT-functionalized crystals.

Crystal structures nonetheless, remain unchanged after incubation of amine-functionalized silica with a blank compound, toluene. TNT functionalization therefore, produced organized structures, while the control DNT produced randomized structures and toluene have no functionalization effect on the —NH$_2$-SiO$_2$ crystals.

The photonic band and band gaps of both the transmission and reflection spectrums from the studied detection range are plotted in Figure 7 (a) and (b), respectively. In these plots, control DNT has zero band edges because of the impossibility of measuring their centre-to-centre distance due to the randomization effect. Higher band edges are labeled as Em' with m = 1,2,3. From the response curves, PB and PBG edges increased with the increasing TNT concentration.
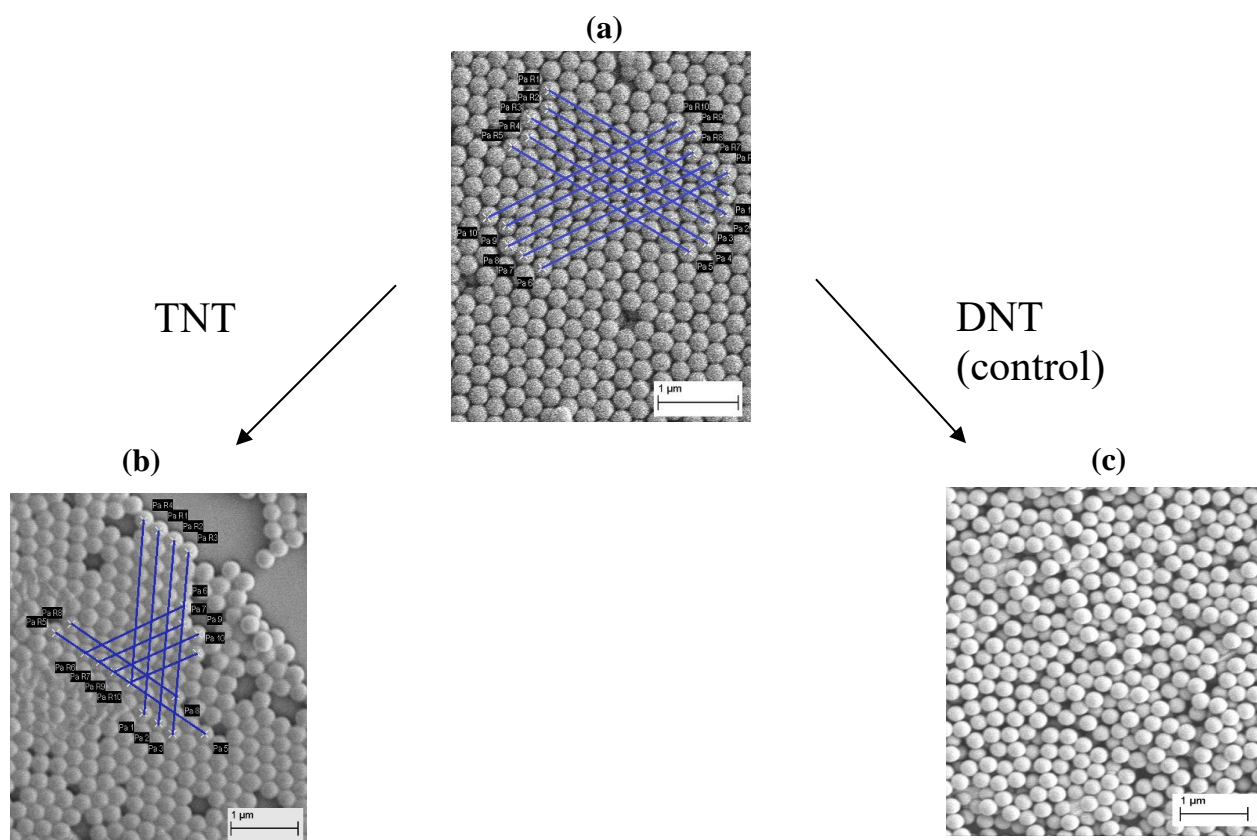
(a)

TNT

DNT
(control)

(b)

(c)

Figure 6. Scanning electron microscopy (SEM) images of (**a**) amine-functionalized silica (—NH$_2$-SiO$_2$) crystals, (**b**) 10^{-4} M TNT- and (**c**) 10^{-4} M DNT-functionalized on the —NH$_2$-SiO$_2$ surfaces.

A third order polynomial fit was used to extract the $\alpha, \beta,$ and γ slope values following the fitting equation: $Energy\ Level = c + \alpha.x^1 + \beta.x^2 + \gamma.x^3$, where c is the intercept, $\alpha, \beta, and\ \gamma$ are the slopes. Table 4 shows a list of the fitting parameters in the method section. Figure 7 shows a monotonic TPBES responses as a function of the TNT concentration. In contrast to the TPBES response, it is evident that the reflection band edges possess larger error bars due to its 'dull' edges.

Since the band edges of the TPBES response behave monotonically, its first order slope, α for both photonic bands and band gaps can be plotted as shown in Figure 8. This is a merit function of the TPBES detection system which proved to be more sensitive than the reflection technique for the same detection range.
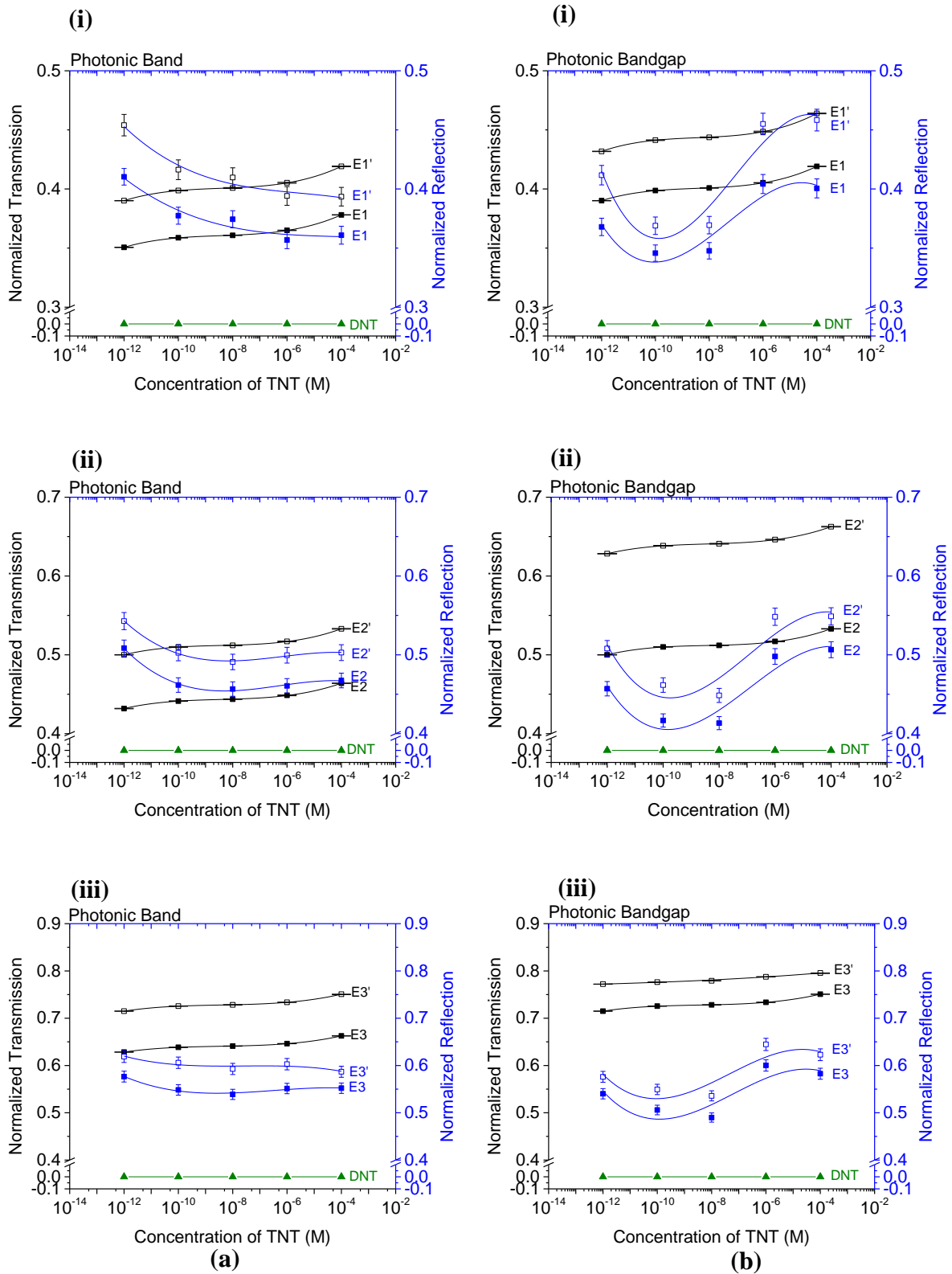
Figure 7: Experimental results of the TPBES response (normalized transmission) and reflection as a function of TNT concentration: (a) photonic band and (b) band gap edges.
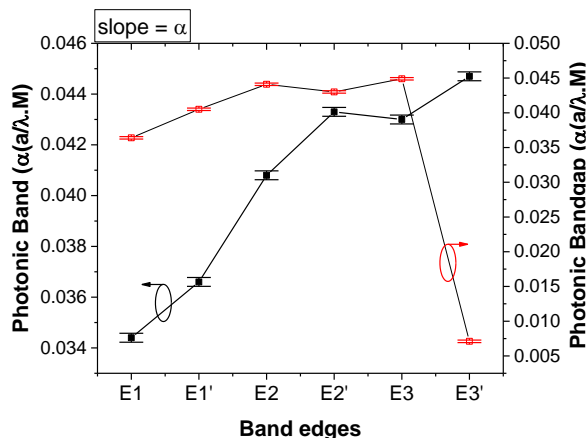
Figure 8. First-order slope, α of photonic band and band gap from third order polynomial fit.

The crystals centre-to-centre distance after TNT functionalization was also examined in solution using a well-established technique known as Zetasizer Nano-ZS, a tool based on dynamic light scattering (DLS). Results of the DLS Intensity Mean (*d.nm*) measurement of the TNT-functionalized crystals at different concentrations is shown in Figure 9. DLS findings validate their agreement with the SEM results.
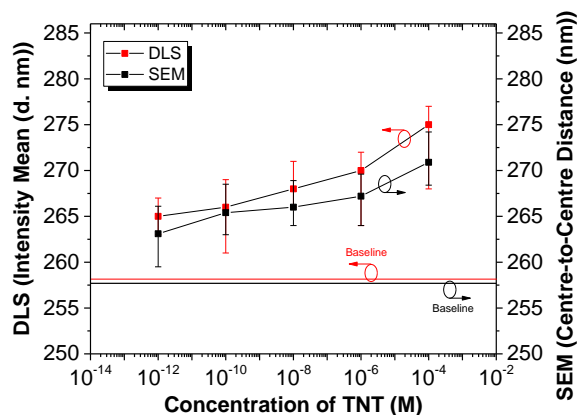
Figure 9. Dynamic light scattering (DLS) and scanning electron microscopy (SEM) results for different TNT concentrations. Toluene blank was used as the baseline for both measurements.

Correlation between (*a*) and n_{eff}. The effective refractive index, n_{eff} depends on the centre-to-centre distance changed based on Equation (1) to (4) in the methods section. The n_{eff} of functionalized crystals in each functionalization state were calculated and are listed in Table 2. Although there is an increased in the centre-to-centre distance of 7.5 nm after amine

11

functionalization, the n_{eff} remained the same as the bare silica. This is because amine functionalization caused decreased in the silica volume fraction from 52.4% to 47.9% to allow the 4.5% volume fraction of amine, within 47.6% volume fraction of ethanol. Based on Equation (1) and an analogous refractive index value for silica and amine of 1.46, resulted in an analogous ε as shown in Table 2.

Table 2. The effective refractive indices n_{eff}, and their corresponding dielectric constant, ε for bare and functionalized silica crystals

	SiO_2	—NH_2	TNT concentrations (M)				
			10^{-12}	10^{-10}	10^{-8}	10^{-6}	10^{-4}
n_{eff}	1.413	1.413	1.419	1.421	1.422	1.424	1.427
ε	1.997	1.997	2.015	2.021	2.023	2.026	2.036

Since DNT crystal structures are randomized, measuring their centre-to-centre distances and hence, their n_{eff} was difficult. On the other hand, TNT functionalization produces n_{eff} changed after attachment of 10^{-12} M. In order to understand the experimental TPBES responses from 10^{-12} M and 10^{-4} M, we run a simulation by utilizing the *(a)* and n_{eff} of 10^{-12} M TNT as baseline with a_o of 263.1 nm and dielectric constant of $\varepsilon_0 = n_{eff}^2 = 1.419^2 \sim 2.015$. COMSOL Multiphysics 5.1 (RF module) was used to simulate the transmission spectra in the 200-800 nm range. Two sets of simulations were performed: the first set involved a parametric sweep of the centre-to-centre distance (*a*) of TNT functionalized crystals varying from 263.1 nm to 270. 9 nm, demonstrated in Table 1, with ε_0 as 2.015, taking the 10^{-12} M dielectric constant presented in from Table 2. The second set involved a parametric sweep of the dielectric constant from 2.015 to 2.036, with a_o as 263.1 nm. The results of the first and second simulations are displayed in Figure 10 (a) and (b), respectively. Insets of Figure 10 (a) and (b) show shifts in both variations but larger photonic bands shift (marked as 1, 2 and 3) are observed in sweeping centre-to-centre distance than the dielectric constants. Thus, the TPBES response is more sensitive to the centre-to-centre distance changed than the contrast of the dielectric constant. From the simulation results, we used the photonic band (PB) edge data to compare with our experimental results.
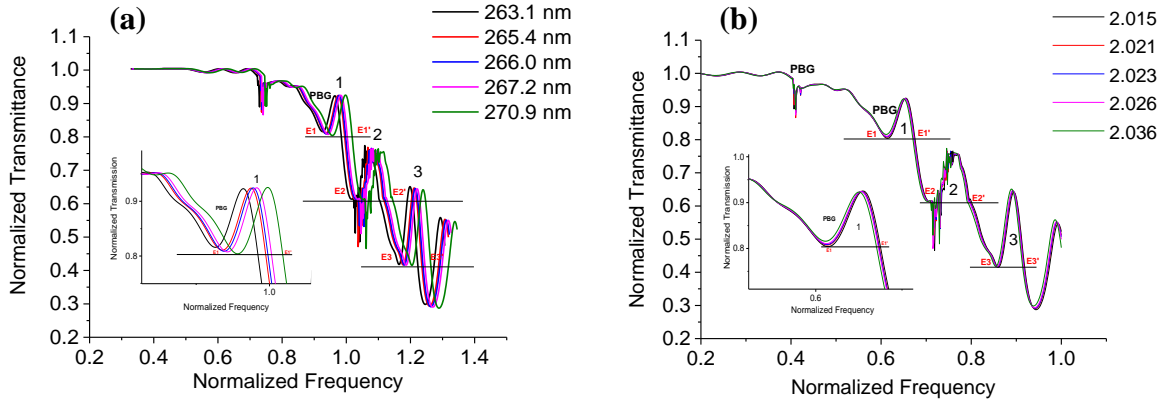
Figure 10. Simulation results of 3D electromagnetic waves in the frequency domains (ewfd) demonstrate (**a**) centre-to-centre distance variations from 263.1 nm to 270. 9 nm, keeping dielectric constant of ε_0 as 2.015, whilst (**b**) dielectric constant variation from 2.015 to 2.036, keeping a_o as 263.1 nm. Photonic band (PB) regions are labeled as 1, 2, and 3 of transmittance peaks.

We extracted the PB information from Figure 10 (a) and (b) and plotted in Figure 11 (a) and (b), respectively. Sweeping (a) produces a positive linear slope of α_n in contrast to negative slope β_n of varying the ε.
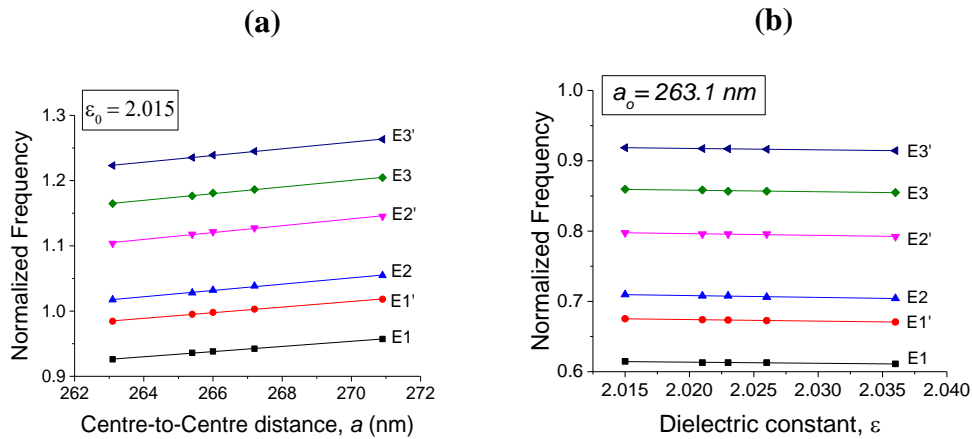

Figure 11. 3D simulation spectroscopy results: The parametric sweep of (**a**) centre-to-centre distance, *(a)* with ε_0 of 2.015, and (**b**) dielectric constant, with a_o as 263.1 nm.

13

Therefore, the centre-to-centre distance and dielectric constant perturbations yield a TPBES response in terms of the (a) and (ε) sweeps as shown in Equation (1):

$$E_n(a_n, \varepsilon_n) = E_0(a_0, \varepsilon_0) + \alpha_n * \left(\frac{\Delta a_n}{a_0}\right) + \beta_n * \left(\frac{\Delta \varepsilon_n}{\varepsilon_0}\right) \tag{1}$$

where $E_0(a_0, \varepsilon_0)$ is the baseline band edge of 10^{-12} M TNT functionalized crystals, $\alpha_n = \alpha * \alpha_0$ and $\beta_n = \beta * \beta_0$ are the slopes from the parametric sweep of centre-to-centre (α) and dielectric (β) obtained in Figure 11 (a) and (b), respectively multiplied with their corresponding baseline slopes of α_0 and β_0. The shifts for different TNT concentrations in terms of the centre-to-centre distance and dielectric changed are $\Delta a_n = a_n - a_0$ and $\Delta \varepsilon_n = \varepsilon_n - \varepsilon_0$, respectively. a_n and ε_n correspond to the centre-to-centre distance and dielectric constant of TNT concentrations where n is the concentration. Respective baseline band edges, slope values of α_n and β_n are listed in Table 3.

Table 3. Baseline band edges, α_n and β_n slope values for each parametric sweeps from the simulation results.

Band edges	$E_0(a_0, \varepsilon_0)$	α_n	β_n
E_1	0.3506	1.03925	-0.31837
$E_{1'}$	0.3901	1.13396	-0.44129
E_2	0.4318	1.26814	-0.52592
$E_{2'}$	0.5000	1.38391	-0.49771
E_3	0.6283	1.34181	-0.44532
$E_{3'}$	0.7149	1.35233	-0.40502

Simulation data listed in Table 3 was used to plot the TPBES responses based on Equation (1) and displayed in Figure 12. The resultant plot is a third-order polynomial fit of $E_n(a_n, \varepsilon_n)$ as described in Equation (2):

$$E_n(a_0, \varepsilon_0) + \alpha_n * \left[\left(\frac{\Delta a_n}{a_0}\right), \left(\frac{\Delta \varepsilon_n}{\varepsilon_0}\right)\right] + \beta_n * \left[\left(\frac{\Delta a_n}{a_0}\right), \left(\frac{\Delta \varepsilon_n}{\varepsilon_0}\right)\right]^2 + \gamma_n * \left[\left(\frac{\Delta a_n}{a_0}\right), \left(\frac{\Delta \varepsilon_n}{\varepsilon_0}\right)\right]^3 \tag{2}$$
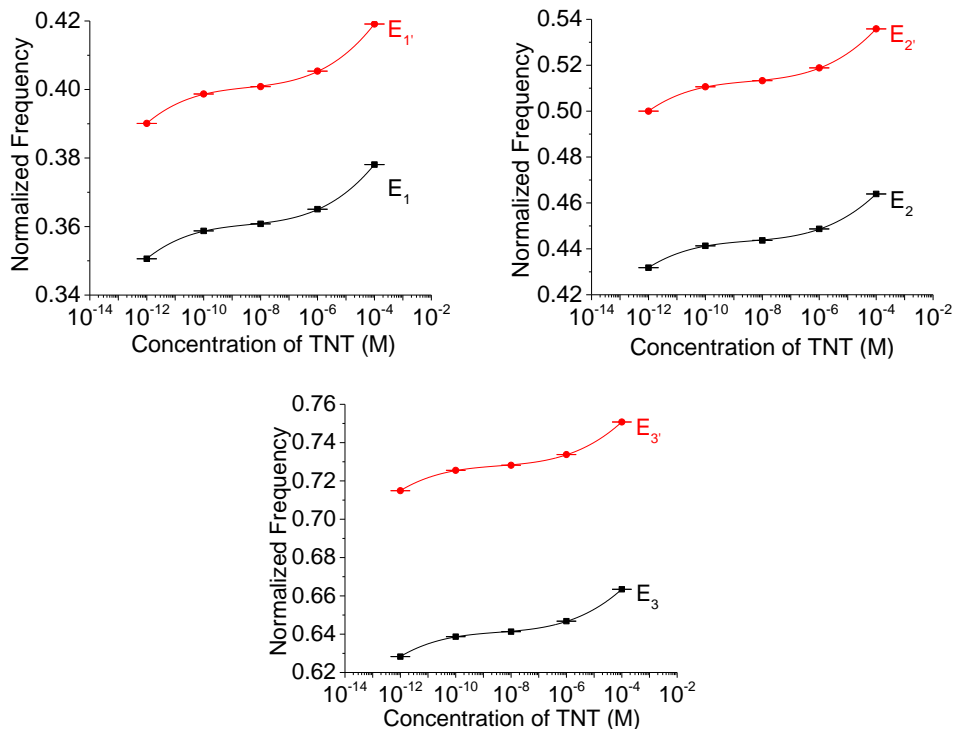
Figure 12. Photonic band edges based on simulation results.

Discussion

We have shown that the simulation results in Figure 12 are in agreement with the experimental results displayed in Figure 7 (a). The advantage of TPBES over the reflection-based results include distinctive sharp edges of photonic bands and full penetration of light through the assembled structures for the bulk properties. The measured TPBES response showed the photonic band edge shifting towards high energy in three stages for different TNT concentrations: a) 1.2-1.6% for 10^{-12} to 10^{-10} M, b) <1% for 10^{-10} to 10^{-6} M and c) 1.6-2% for 10^{-6} to 10^{-4} M. This behavior was simulated by using the centre-to-centre distance (a_n) between the assembled particles and effective dielectric constant (ε_n) as a function of the TNT concentrations. The high sensitivity of TPBES response towards TNT functionalization at low concentration of 10^{-12} M may be attributed to the combined effect of the high surface area-to-volume ratio of the functionalized nano particles in use and the full penetration of the light through the assembled structure, which helped to expand the dynamic range of the detection. This work describes a highly sensitive approach to detect TNT explosives. The method is convenient and it can be incorporated easily into microfluidic systems.

15

Conclusion

Photonic crystals (PhCs) possess outstanding optical properties that can be exploited for chemical sensing. We reported a simple, sensitive and label-free method for sensing 2,4,6-trinitrotoluene (TNT) utilizing a three-dimensional close-packed PhC structure made of functionalized amorphous silica (SiO_2) nano particles. It consists of alternating high and low refractive index regions and has optical properties such as photonic band structures very sensitive to the change of physical structures. This study offers a detection method based on the transmissive photonic band edge shift (TPBES) due to the binding of 2,4,6-trinitrotolune (TNT) with amine anchored on particle surfaces. Surface functionalization was performed by first anchoring amine ($—NH_2$) head groups from 3-aminopropyl-triethoxysilane as bioreceptors that specifically bind with a TNT target to form Meisenheimer complexes. Due to the surface functionalization, the separation between the close-packed particles measured by scanning electron microscopy increases from state 1 to 3. The increase of TNT concentrations from 10^{-12} M to 10^{-4} M will further increase the effective particle separation and change the contrast of refractive index. A wide detection range of TNT concentrations was used and successfully detected from 10^{-12} M to 10^{-4} M together with 2,4-dinitritoluene (DNT) and toluene as control and blank, respectively. The TPBES system is very selective towards TNT even though the chemical structure of TNT and DNT are relatively similar. This is because functionalization of TNT further increased the effective particle separation (a) and change the contrast of the refractive index (n_{eff}) which resulted in the PB and PBG edge shifts. Successful detection of TNT is caused by a periodic arrangement of the functionalized crystals. An incomplete reaction between DNT and $—NH_2$-SiO_2 crystals resulted in randomization of self-assembly structure. This randomization effect resulted in decreasing signals of TPBES response with no distinctive photonic bands and band gaps. This detection method reveals sharp band edges than reported in our previous findings[44] with full penetration of light through the three-dimensional self-assembly structure. Smaller measurement errors with comprehensive information such as the changed of particles distance and dielectric constant in comparison to the reflection method are the TPBES figure of merit. This method presents a convenient tool for sensing as the effect can be made specific between TNT and amine head group. Future study on other relative explosives with similar structures, such as nitrobenzene (NB), 2-nitrotoluene (2-NT), 4-nitrophenol (4-NP), or in the real samples, will help to reveal the range of explosives this detection method can apply.

Methods

Amine Functionalization. The SiO_2 crystals suspension was prepared in anhydrous ethanol via solvent replacement method. First, water suspension was evaporated to dryness then followed by addition of ethanol using these parameters: 4000 rpm centrifugation speed for 5 minutes, and sonication for 10 minutes, three times. The SiO_2 crystals suspended in ethanol was chemically functionalized in a solution of 18.2 MΩ-cm Millipore water, ammonium water (NH_4OH) and pure ethanol. The mixture was stirred in a flask placed on a hotplate and 5mM APTES was slowly stirred into the flask for 6 hours at 60°C. After 6 hours of continuous stirring, the hot plate was turned off with further stirring for 30 minutes, and left overnight. The amine-functionalized SiO_2 crystals (—NH_2-SiO_2) then went through a series of solvent replacement method until the crystals were fully dispersed in pure ethanol giving a milky or hazy appearance. Spectrophotometric detection of amines was made by reacting 10^{-4} M p-benzoquinone reagent with various concentrations of amines. The —NH_2-SiO_2 suspensions were diluted 7 times and reacted with 10^{-4} M p-benzoquinone. By using UV-NIR absorption spectra scanned from 190 nm to 1100 nm, it was estimated that $1.727 \ x \ 10^{14}$ reactive sites of primary amine were functionalized on the silica crystal surfaces.

TNT Functionalization. TNT binding with the amine head group was done following the method performed by Ho *et al.*[62] Range of TNT and DNT concentrations:10^{-12}, 10^{-10}, 10^{-8}, 10^{-6} and 10^{-4} M were examined. DNT and toluene in acetonitrile were used as control and blank, respectively. Since acetonitrile is immiscible with water-based buffer 10mM HEPES + 150 mM NaCl, the solvent was left to dry in a fume cupboard for 2 hours. Pure ethanol was added to the explosives thus makeup to the total volume of 50 µL. During the drying of acetonitrile, 5.54 µL of —NH_2-SiO_2 crystals suspended in ethanol was mixed with 200 µL of 10 mM HEPES + 150 mM NaCl for approximately 2 hours. 50 µL of various TNT concentrations in pure ethanol is then added to saturated —NH_2-SiO_2 crystals suspended in 10 mM HEPES + 150 mM NaCl and incubated for one hour with minimal shaking using a vortex machine. TNT functionalization on —NH_2-SiO_2 crystals surfaces was obtained after centrifugation at 2000 rpm for 90 seconds followed by three times washing with pure ethanol.

Self-Assembly of Functionalized Crystals. The TNT functionalized crystals were self-assembled in solution for the TPBES response. 500 µL of the TNT-functionalized silica crystals were self-assembled over two weeks in a 1-cm quartz cuvette but by shaking the cuvette could rapid the self-assembly process. For the SEM measurement of the centre-to-centre distance (a) of the functionalized crystals; 50 µL of TNT-functionalized crystals were self-assembled on a quartz substrate via solvent evaporation technique in ambient temperature, for 48 hours. 3 cm x 0.1 cm quartz substrates were cleaned with acetone and IPA for 15 minutes each in an ultrasonic bath and blow dry with nitrogen gun before use.

Spectrometric measurement. To quantify the transmissive photonic band edge shift of the three-dimensional self-assembled crystals in solution, using Jasco V-670 and its spectra measurement software. Spectronic GENESYS 6 (UV-NIR Spectrophotometer) by Thermo Electron Corporation and Thermo Scientific™ VISIONlite™ software were used to measure the concentration of primary amine on silica surfaces.

Scanning Electron Microscopy. Used to examine the center-to-center distance, (*a*) and to distinguish the crystals structure after modification with APTES, and TNT. Films were sputtered with gold at 55mA, for 15 seconds before measurement with a coating thickness of approximately 14 nanometers. SEM imaging analysis was done at a low accelerating voltage of 3kV using Zeiss Scanning Electron Microscopy, with SmartSEM imaging software.

PeakFit v4.12 Automated Peak Separation Analysis Software. Used to resolve multiple peak wavelengths.

Zetasizer Nanoscience Nano-ZS by Malvern Instruments. Used to determine the particle size in solution after functionalization. Different concentrations of explosive functionalized crystals were measured in dispersant of pure ethanol with a refractive index of 1.361, and viscosity of 1.2 millipascal-second at 20° Celsius. Silica with a refractive index of 1.45 and absorption of 0.001 was used as the material. The particle sizing was measured at 173° Backscatter (NIBS default).

Simulation. Used COMSOL 5.1 (RF module), under periodic boundary conditions to simulate a three-dimensional structure of a device consisting of 250 nm silica nanoparticle embedded in amine surrounded by TNT molecules and ethanol sitting on a quartz substrate. In our simulation,

we used a two-dimensional approximation of our silica nanoparticle as seen by the incident broadband light from 200 nm to 800 nm and obtain its transmission spectra. Two sets of simulations were performed: the first set involved a parametric sweep of the centre-to-centre distance (a) of the TNT functionalized crystals which define the thickness of the TNT layer from 263.1 nm to 270. 9 nm, with $\varepsilon_0 = 2.015$. The second set involved a parametric sweep of the dielectric constant from 2.015 to 2.036, with a_o as 263.1 nm.

Effective Refractive Index Calculation. The effective refractive index (n_{eff}) changed due to the organic ligands binding on the crystal surfaces, is calculated as[63-64]:

$$n_{eff} = \sqrt{n^2_{Silica}\, f_{Silica} + n^2_{Amine} f_{Amine} + n^2_{TNT} f_{TNT} + n^2_{Ethanol} f_{Ethanol}} \qquad (3)$$

where n_{eff} is the effective refractive index, n_{Silica} 3, n_{Amine}, n_{TNT} and $n_{Ethanol}$ are the refractive indices (RI) of the silica, amine, TNT, and ethanol, respectively. RI of silica and amine are 1.46; TNT and ethanol are 1.65 and 1.36 respectively. f_{Silica}, f_{Amine}, f_{TNT}, and $f_{Ethanol}$ are the respective volume fractions of silica, amine, TNT and ethanol.[65-67] The volume fraction of the crystal is given as $\frac{\pi}{6} \approx 0.524$. This means that the surrounding medium of ethanol has a volume fraction, $f_{ethanol} = 1 - 0.524 = 0.476$.

Thus the total volume fraction (f_{Total}) of functionalized crystals is equivalent to 0.524 as described in Equation (4). Amine functionalization resulted in a constant volume fraction, $f_{Amine} = 0.045$ for all TNT concentrations.

$$0.524 = f_{Silica} + f_{Amine} + f_{TNT} = \frac{4\pi}{3} \times (r + L_{Amine} + L_{TNT})^3 \qquad (4)$$

where r is the radius of the silica crystals, L_{Amine} and L_{TNT} are the amine and TNT functionalized lengths as illustrated in Scheme 1, respectively. Amine and TNT lengths were calculated using Equation (5) where a_0, a_1 and a_2 corresponds to the respective centre-to-centre distance of bare silica, amine and TNT-functionalized crystals.

$$L_{Amine} = \frac{a_1 - a_0}{2} \qquad L_{TNT} = \frac{a_2 - a_1}{2} \qquad\qquad (5)$$
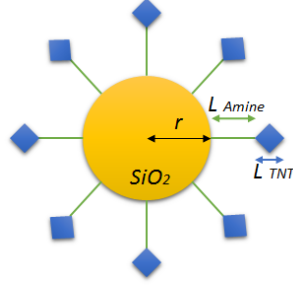
Scheme 1. Schematic illustration of ligands binding on the surface of bare silica (SiO_2) cry5stal with radius, r. L_{Amine} and L_{TNT} represent amine and TNT functionalized lengths, respectively. Therefore, n_{eff} can be computed using Equation (1) by inserting $f_{Amine} = 0.045$, $f_{Ethanol} = 0.476$, f_{Silica} and f_{TNT} calculated following Equation (6) and respective refractive indices.

$$f_{Silica} = \frac{\frac{4\pi}{3} \times (r)^3}{8 \times (r + L_{Amine} + L_{TNT})^3} \quad \text{and}$$

$$V_{TNT} = 0.524 - (f_{Silica} + f_{Amine}) \qquad\qquad (6)$$

Materials. Silica nanoparticles suspension with diameter size of 240 ± 10 nm stock concentrati6on of 30% (w/v) in water was purchased from Dongjian Biological (China); 18.2 MΩ-cm Millipore water, ammonium hydroxide solution (NH_4OH) 28% NH_3 in H_2O, (≥99.99% trace metals basis); anhydrous ethanol (EtOH) (>99.9%); acetonitrile (anhydrous, 99.8%), cleaning solvent such as acetone and isopropyl alcohol (IPA); APTES (99%); p-benzoquinone for spectrophotometric detection of amines, ≥99.5% (HPLC); 10mM HEPES + 150 mM NaCl, HEPES solution (1 M, pH 7.0-7.6) and Sodium Chloride (NaCl) were purchased from Sigma-Aldrich. 2,4,6-Trinitrotoluene and 2,4-dinitrotoluene solutions (1000 µg/mL in acetonitrile) were obtained from Defence Science and Technology Laboratory (DSTL); quartz substrate of 3 cm x 0.1 nm purchased from Pi-KEM - Spectrosil B Polished Windows/Quartz with a thickness of 1.25 mm and diameter of 24.6 ± 0.10 mm.

Transmission and Reflection Slopes. Third order polynomial fit equation: $Energy\ Level = c + \alpha x^1 + \beta x^2 + \gamma x^3$. Where c is the intercept, $\alpha, \beta, and\ \gamma$ are the slopes. R^2 is the R squared. T and R are transmission and reflection, respectively.

Table 4: Third-order polynomial fitting values for transmission (T) and reflection (R) responses of the (i) photonic band and (ii) photonic band gap.

Photonic Band edges	Intercept		$\propto$		β		γ	
	T	R	T	R	T	R	T	R
E_1	0.4622	0.3508	0.0344	-0.0052	0.0040	-0.0011	1.562E-4	-9.0596E-5
$E_1{}'$	0.5085	0.3582	0.0366	-0.0165	0.0042	-0.0026	1.6638E-4	-1.5653E-4
E_2	0.5636	0.3900	0.0408	-0.0435	0.0047	-0.0077	1.8570E-4	-4.064E-4
$E_2{}'$	0.6385	0.4390	0.0433	-0.0367	0.0050	-0.0066	1.9821E-4	-3.5484E-4
E_3	0.7678	0.4870	0.0430	-0.0361	0.0050	-0.0062	1.9540E-4	-3.1773E-4
$E_3{}'$	0.8600	0.4830	0.0447	-0.0466	0.0052	-0.0062	2.0319E-4	-2.7081E-4

(i)

Photonic Band gap edges	Intercept		$\propto$		β		γ	
	T	R	T	R	T	R	T	R
E_1	0.5082	0.1878	0.0364	-0.1123	0.0042	-0.0179	1.6541E-4	-8.1726E-4
$E_1{}'$	0.5629	0.1911	0.0405	-0.1493	0.0047	-0.0251	1.8430E-4	-0.0012
E_2	0.6403	0.2926	0.0441	-0.1261	0.0051	-0.0222	2.0243E-4	-0.0011
$E_2{}'$	0.7679	0.2879	0.0430	-0.1501	0.0050	-0.0258	1.9558E-4	-0.0012
E_3	0.8605	0.2433	0.0449	-0.1818	0.0052	-0.0292	2.0361E-4	-0.0014
$E_3{}'$	0.8190	0.2645	0.0071	-0.1876	3.4770E-4	-0.0295	6.6416E-6	-0.0013

(ii)

AUTHOR INFORMATION

Author Contributions

The manuscript and all of the experimental work were done by Noorhayati Idros. Man Yi Ho was responsible for the idea of testing explosives while Varun Kamboj was responsible for the simulation work. Hua Xu helped with the chemistry of APTES attachment on silica nanoparticles. ZhongZe Gu supplied the nanoparticles and introduced the use of the silica nanoparticles. Harvey Beere and David Ritchie were involved in the COMSOL modeling along with Varun Kamboj in analyzing and discussing the results of the simulations. Daping Chu supervised the work, advised the paper presentation and contents, and participated in the paper writing. Daping Chu also suggested the use of transmission photonic band edge for its sharpness. All authors have given approval to the final version of the manuscript.

ASSOCIATED CONTENT

Supporting Information Available: The Supporting Information is available free of charge on the ACS Publications *via* the Internet at http://pubs.acs.org.

References

1. Fenzl, C.; Hirsch, T.; Wolfbeis, O.S. Photonic Crystals for Chemical Sensing and Biosensing. *Angew. Chem. Int. Ed*. **2014**, *53*, 3318 – 3335.

2. Joannopoulos, J.D.; Johnson, S.G.; Winn, J.N.; Meade, R.D. Photonic Crystals: Molding the Flow of Light, 2nd ed., *Princeton University Press*, Princeton, **2008**.

3. Yablonovitch, E. Inhibited spontaneous emission in solid-state physics and electronics. *Phys. Rev. Lett.* **1987**, *58*, 2059–2062.

4. John, S. Strong localization of photons in certain disordered dielectric superlattices. *Phys. Rev. Lett.* **1987**, *58*, 2486–2489.

5. Lotsch, B.V.; Ozin, G.A. Photonic Clays: A New Family of Functional 1D Photonic Crystals. *ACS Nano* **2008**, *2*, 2065–2074.

6. Lotsch, B.V.; Ozin, G.A. Clay Bragg Stack Optical Sensors. *Adv. Mater.* **2008**, *20*, 4079–4084.

7. Wang, Z.; Zhang, J.; Xie, J.; Yin, Y.; Wang, Z.; Shen, H.; Li, Y.; Li, J.; Liang, S.; Cui, L.; Zhang, L.; Zhang, H.; Yang, B. Patterning Organic/Inorganic Hybrid Bragg Stacks by Integrating One-Dimensional Photonic Crystals and Macrocavities through Photolithography: Toward Tunable Colorful Patterns as Highly Selective Sensors. *ACS Appl. Mater. Interfaces* **2012**, *4*, 1397–1403.

8. Ouyang, H.; Fauchet, P.M. Biosensing using Porous Silicon Photonic Bandgap Structures. *SPIE Optics East* **2005**.

9. Kim, S.-H.; Lim, J.-M.; Lee, S.-K.; Heo, C.-J.; Yang, S.-M. Biofunctional colloids and their assemblies. *Soft Matter.* **2010**, *6*, 1092–1110.

10. Kim, S.-H.; Lee, S. Y.; Yang, S.-M.; Yi, G.-R. Self-assembled colloidal structures for photonics. *NPG Asia Mater.* **2011**, *3*(1), 25–33.

11. Ge, J.; Yin, Y. Responsive Photonic Crystals. *Angew. Chem. Int. Ed.* **2011**, *50*, 1492–1522.

12. Iler, R.K. The Chemistry of Silica: Solubility, Polymerization, Colloid and Surface Properties and Biochemistry of Silica, *Wiley, New York,* **1979**.

13. Stöber, W.; Fink, A.; Bohn, E. Controlled Growth of Monodisperse Silica Spheres in the Micron Size Range. *J. Colloid Interface Sci.* **1968**, *26*, 62–69.

14. Matijevic, E. Uniform inorganic colloid dispersions. Achievements and challenges. *Langmuir* **1994**, *10*(1), 8–16.

15. Im, S.H.; Lim, Y.T.; Suh, D.J.; Park, O.O. Three-Dimensional Self-Assembly of Colloids at a Water–Air Interface: A Novel Technique for the Fabrication of Photonic Bandgap Crystals. *Adv. Mater.* **2002**, *14*, 1367–1369.

16. Nishijima, Y.; Ueno, K.; Juodkazis, S.; Mizeikis, V.; Misawa, H.; Tanimura, T.; Maeda, K. Inverse silica opal photonic crystals for optical sensing applications. *Opt. Express* **2007**, *15*(20), 12979–12988.

17. Aguirre, C.I.; Reguera, E.; Stein, A. Colloidal Photonic Crystal Pigments with Low Angle Dependence. *ACS Appl. Mater. Interfaces* **2010**, *2*, 3257–3262.

18. Cai, Z.; Liu, Y.J.; Teng, J.; Lu, X. Fabrication of Large Domain Crack-Free Colloidal Crystal Heterostructures with Superposition Bandgaps Using Hydrophobic Polystyrene Spheres. *ACS Appl. Mater. Interfaces* **2012**, *4*, 5562–5569.

19. Marlow, F.; Muldarisnur, Sharifi, P.; Brinkmann, R.; Mendive, C. Opals: Status and Prospects. *Angew. Chem. Int. Ed.* **2009**, *48*, 6212–6233. DOI: 10.1002/anie.200900210.

20. Galisteo-López, J.F.; Ibisate, M.; Sapienza, R.; Froufe-Pérez, L.S.; Blanco, A.; López, C. Self-Assembled Photonic Structures. *Adv. Mater.* **2011**, *23*, 30–69.

21. Ouyang, H.; Fauchet, P. M. Biosensing using Porous Silicon Photonic Bandgap Structures. *SPIE Opt. East* **2005**.

22. Corma, A. From microporous to mesoporous molecular sieve materials and their use in catalysis. *Chem. Rev.* **1997**, *97*, 2373–2419.

23. Ciesla, U.; Schüth, F. Ordered mesoporous materials. *Microporous Mesoporous Mater.* **1999**, *27*, 131–149.

24. Hartmann, M. Ordered mesoporous materials for bioadsorption and biocatalysis. *Chem. Mater.* **2005**, *17*, 4577–4593.

25. Øye, G.; Glomm, W.R.; Vrålstad, T.; Volden, S.; Magnusson, H.; Stöcker, M.; Sjöblom, J. Synthesis, functionalisation and characterisation of mesoporous materials and sol-gel glasses for applications in catalysis, adsorption and photonics. *Adv. Colloid Interface Sci.* **2006**, 123–126.

26. Wan, Y.; Zhao, D. On the controllable soft-templating approach to mesoporous silicates. *Chem. Rev.* **2007**, *107*, 2821–2860.

27. Sanchez, C.; Boissière, C.; Grosso, D.; Laberty, C.; Nicole, L. Design, synthesis, and properties of inorganic and hybrid thin films having periodically organized nanoporosity. *Chem. Mater.* **2008**, *20*, 682–737.

28. Manzano, M.; Vallet-Regi, M. New developments in ordered mesoporous materials for drug delivery. *J. Mater. Chem.* **2010**, *20*, 5593–5604.

29. Ren, Y.; Ma, Z.; Bruce, P.G. Ordered mesoporous metal oxides: Synthesis and applications. *Chem. Soc. Rev.* **2012**, *41*, 4909–4927.

30. Möller, K.; Kobler, J.; Bein, T. Colloidal Suspensions of Nanometer-Sized Mesoporous Silica. *Adv. Funct. Mater.* **2007**, *17*, 605–612.

31. Toal, S.J.; Magde, D.; Trogler, W.C. Luminescent oligo(tetraphenyl)silole nanoparticles as chemical sensors for aqueous TNT. *Chem. Commun.* **2005**, *43,* 5465–5467.

32. Salinas, Y.; Agostini, A.; Perez-Esteve, E.; Martinez-Manez, R.; Sancenon, F.; Dolores Marcos, M.; Soto, J.; Costero, A.M.; Gil, S.; Parra, M.; Amoros, P. Fluorogenic detection

of Tetryl and TNT explosives using nanoscopic-capped mesoporous hybrid materials. *J. Mater. Chem. A* **2013**, *1*, 3561–3564.

33. Salinas, Y.; Solano, M.V.; Sørensen, R.E.; Larsen, K.R.; Lycoops, J.; Jeppesen, J.O.; Martínez-Máñez, R.; Sancenón, F.; Dolores Marcos, M.; Amorós, P.; *Guillem, C.* Chromo-Fluorogenic Detection of Nitroaromatic Explosives by Using Silica Mesoporous Supports Gated with Tetrathiafulvalene Derivatives. *Chem. Eur. J.* **2014**, *20*, 855–866.

34. Xu, S.; Lu, H. Mesoporous structured MIPs@CDs fluorescence sensor for highly sensitive detection of TNT. *Biosens. Bioelectron.* **2016**, *85*, 950-956.

35. Liu, M.; Chen, W. Graphene nanosheets-supported Ag nanoparticles for ultrasensitive detection of TNT by surface-enhanced Raman spectroscopy. *Biosens. Bioelectron.* **2013**, *46*, 68-73.

36. Pandya, A.; Goswami, H.; Lodha, A.; Menon, S. K. A novel nanoaggregation detection technique of TNT using selective and ultrasensitive nanocurcumin as a probe. *Analyst* **2012**, *137*, 1771–1774.

37. Senesac, L.; Thundat, T.G. Nanosensors for trace explosive detection. *Materials Today* **2008**, *11*, 28–36.

38. Wynn, C.M.; Palmacci, S.; Kunz, R. R.; Rothschild, M. A Novel Method for Remotely Detecting Trace Explosives. *SPIE Newsr.* **2008**, doi:10.1117/2.1200805.1179.

39. Colton, R.J.; Russell, J.N. Counterterrorism. Making the world a safer place. *Science* **2003**, *299*, 1324–1325.

40. Hallowell, S.F. Screening people for illicit substances: A survey of current portal technology. *Talanta* **2001**, *54*, 447–458.

41. Fainberg, A. Explosives Detection for Aviation Security. *Science* **1992**, *255*, 1531–1537.

42. Lubin, A.A.; Plaxco, K.W. Folding-based electrochemical biosensors: The case for responsive nucleic acid architectures. *Acc. Chem. Res.* **2010**, *43*, 496–505.

43. Smith, K.D.; McCord, B.R.; MacCrehan, W.A.; Mount, K.; Rowe, W.F. Detection of smokeless powder residue on pipe bombs by micellar electrokinetic chromatography. *J. Forensic Sci.* **1999**, *44*, 789–794.

44. Thomas, S.W. III; Joly, G.D.; Swager, T. M. Chemical Sensors Based on Amplifying Fluorescent Conjugated Polymers. *Chem. Rev.* **2007**, *107*, 1339–1386.

45. Dillewijn, P.V.; Couselo, J.L.; Corredoira, E.; Delgado, A.; Wittich, R.M.; Ballester, A.; Ramos, J.L. Bioremediation of 2,4,6-trinitrotoluene by bacterial nitroreductase expressing transgenic aspen. *Environ. Sci. Technol.* **2008**, *42*, 7405–7410.

46. Brettell, T.A.; Butler, J.M.; Almirall, J.R. Forensic Science. *Anal. Chem.* **2007**, *79*, 4365–4384.

47. McQuade, D.T.; Pullen, A.E.; Swager, T.M. Conjugated polymer-based chemical sensors. *Chem. Rev.* **2000**, *100*, 2537–2574.

48. Samuel, S.R.D.; Dulal, S.; Anant, K.S.; Yerramilli, A.; Hongtao, Y.; Paresh, C.R. A Highly Sensitive and Selective Dynamic Light Scattering Assay for TNT Detection Using p-ATP Attached Gold Nanoparticle. *ACS Appl. Mater. Interfaces* **2010**, *2*, 3455–3460.

49. Bradley, P.M.; Chapelle, F.H.; Factors affecting microbial 2,4,6-trinitrotoluene mineralization in contaminated soil. *Environ. Sci. Technol.* **1995**. *29*, 802–806.

50. Idros, N.; Ho, M.Y.; Pivnenko, M.; Qasim, M.M.; Xu, H.; Gu, Z.; Chu, D. Colorimetric-Based Detection of TNT Explosives Using Functionalized Silica Nanoparticles. *Sensors* **2015**, *15,* 12891-12905.

51. Engel, Y.; Elnathan, R.; Pevzner, A.; Davidi, G.; Flaxer, E.; Patolsky, F. Supersensitive Detection of Explosives by Silicon Nanowire Arrays. *Angew. Chem. Int. Ed.* **2010**, *49*, 6830-6835.

52. Bernasconi, C. F. Kinetic and Spectral Study of Some Reactions of 2,4,6-Trinitrotoluene in Basic Solution. I. Deprotonation and Janovsky Complex Formation. *J. Org. Chem.* **1971**, *36*, 1671-1679.

53. Feng, L.; Li, H.; Qu, Y.; Lu, C. Detection of TNT based on conjugated polymer encapsulated in mesoporous silica nanoparticles through FRET. *Chem. Commun.,* **2012**, *48*, 4633–4635.

54. Zhao, Y.; Shang, L.; Cheng, Y.; Gu, Z. Spherical Colloidal Photonic Crystals. *Acc. Chem. Res.* **2014**, *47*, 3632−3642.

55. Ye, B.; Ding, H.; Cheng, Y.; Gu, H.; Zhao, Y.; Xie, Z.; Gu, Z. Photonic crystal microcapsules for label-free multiplex detection. *Adv. Mater.* **2014**, *26*, 3270–3274.

56. Zhao, Y.; Zhao, X.; Tang, B.; Xu, W.; Li, J.; Hu, J.; Gu, Z. Quantum-Dot-Tagged bioreseptors hydrogel suspension array for multiplex label-free DNA detection. *Adv. Funct. Mater.* **2010**, *20*, 976–982.

57. Zhao, Y.; Zhao, X.; Tang, B.; Xu, W.; Gu, Z. Rapid and sensitive biomolecular screening with encoded macroporous hydrogel photonic beads. *Langmuir* **2010**, *26(9),* 6111–6114.

58. Zhao, X.; Cao, Y.; Ito, F.; Chen, H.; Nagai, K.; Zhao, Y.; Gu, Z. Colloidal crystal beads as supports for biomolecular screening. *Angew. Chem. Int. Ed.* **2006**, *45*, 6835 –6838.

59. Davis, K. E.; Russel, W. B.; Glantschnig, W. J. Disorder-to-order transition in settling suspensions of colloidal silica: X-ray measurements. *Science* **1989**, *245*, 507–510.

60. Fan, W.; Chen, M.; Yang, S.; Wu, L. Centrifugation-assisted assembly of colloidal silica into crack-free and transferable films with tunable crystalline structures. *Sci. Rep.* **2015**, *5,* 12100.

61. Zhou, J.; Wang, J.; Huang, Y.; Liu, G.; Wang, L.; Chen, S.; Li, X.; Wang, D.; Song, Y.; Jiang, L. *Large-area crack-free single-crystal photonic crystals via combined effects of polymerization-assisted assembly and flexible substrate. NPG Asia Mater*. **2012**, *4*, 21–27.

62. Ho, M.Y.; D'Souza, N.; Migliorato, P. Electrochemical Aptamer-Based Sandwich Assays for the Detection of Explosive. *Anal. Chem.* **2012**, *84*, 4245–4247.

63. Gonzalez-Urbina, L., Baert, K., Kolaric, B., Perez-Moreno, J. & Clays, K. Linear and nonlinear optical properties of colloidal photonic crystals. *Chem. Rev*. **2012**, *112*, 2268-2285.

64. Lee, S. Y.; Lee, S-K.; Park, T. J.; Yang, S-M. Method for fabricating photonic-fluidic biosensors using functionalized photonic crystals. WO2007139283 A1, 6 Dec 2007.

65. Fudouzi, H. J. Fabricating high-quality opal films with uniform structure over a large area. *Colloid Interface Sci.* **2004**, *275*, 277 – 283.

66. Lee Y.-J.; Braun, P. V. Tunable Inverse Opal Hydrogel pH Sensors. *Adv. Mater.* **2003**, *15*, 563 – 566.

67. Aguirre, C. I.; Reguera, E.; Stein, A. Tunable Colors in Opals and Inverse Opal Photonic Crystals. *Adv. Funct. Mater.* **2010**, *20*, 2565 – 2578.